ELSEVIER

NeuroImage

www.elsevier.com/locate/ynimg
NeuroImage 27 (2005) 222 – 230

# On-line automatic slice positioning for brain MR imaging ☆

André J.W. van der Kouwe,[a,*] Thomas Benner,[a] Bruce Fischl,[a,b] Franz Schmitt,[c] David H. Salat,[a] Martin Harder,[c] A. Gregory Sorensen,[a] and Anders M. Dale[a,d]

[a]*Department of Radiology, MGH, Athinoula A. Martinos Center for Biomedical Imaging, Room 2301, Building 149, 13th Street, Charlestown, MA 02129, USA*
[b]*MIT AI Laboratory, Cambridge, MA 02139, USA*
[c]*Siemens Medical Solutions, Erlangen, Germany*
[d]*Department of Neurosciences, University of California at San Diego, La Jolla, CA 92093, USA*

Received 12 January 2005; revised 14 March 2005; accepted 31 March 2005
Available online 10 May 2005

**In clinical brain MR imaging protocols, the technician collects a quick localizer and manually positions the subsequent scans using the localizer as a guide. We present a method for automatic slice positioning using a rapidly acquired 3D localizer. The localizer is automatically aligned to a statistical atlas representing 40 healthy subjects. The atlas contains the probability of a given tissue type occurring at a given location in atlas space and the conditional probability distribution of the multi-spectral MRI intensity values for a given tissue class. Accurate rigid alignment of each subject to an atlas ensures that all patients' scans are acquired in a consistent manner. A further benefit is that slices are positioned consistently over time, so that scans of patients returning for follow-up imaging can be compared side-by-side to accurately monitor the progression of illness. The procedure also helps ensure that left/right asymmetries reflect true anatomy rather than being the result of oblique slice positioning relative to the underlying anatomy. The use of an atlas-based procedure eliminates the need to refer to a database of previously scanned images of the same patient and ensures corresponding alignment across scanners and sites, without requiring fiducial markers. Since the registration method is probabilistic, the registration error tends to increase smoothly in the presence of increasing noise and unusual anatomy or pathology rather than failing catastrophically. Translations and rotations relative to the atlas can be set so that planning can be done in anatomical space, rather than scanner coordinates, and stored as part of the protocol allowing standardization of slice orientations.**
**© 2005 Elsevier Inc. All rights reserved.**

*Keywords:* MR imaging; Slice positioning; Atlas-based alignment

## Introduction

We present an automatic prospective method for prescribing MRI slice positions in the brain. Precise and consistent alignment of scans is useful in research as well as in clinical practice to the radiologist reading scans on a daily basis. Precise alignment implies that scans are collected exactly orthogonal to the midline so that observed asymmetries reflect true anatomy and are not simply due to inaccurate scan prescription. Consistent alignment implies that all patients are scanned in the same way and can be compared side-by-side as far as possible given the natural variance in brain anatomy. Most importantly, if the same subject is scanned during multiple scanning sessions, consistent alignment implies that brain pathology can be tracked accurately and progress over time can be quantified. This has application in tracking lesions in multiple sclerosis (Molyneux et al., 1998), tumors, stroke, and other anatomically apparent neuropathologic symptoms (Freeborough et al., 1996). Standardized alignment is particularly useful when voxels are highly anisotropic, as is typical of clinical scans. Our method will aid the MR technologist in completing routine clinical studies in as short a time as possible, while minimizing inadvertent errors and inconsistencies in alignment between subjects.

A method for automatically setting the scan prescription was proposed by Itti et al. (2001). Their method requires a single volume scan, and their algorithm applies a segmentation to find the brain surface. A transformation matching this to a reference surface is found. Orientation differences between subject and

☆ Statement of conflicts of interest: AD is Chief Scientific Advisor and equity holder in CorTechs Laboratories, which has developed atlas-based alignment software used for automatic slice positioning for MRI. The technology described and evaluated in this manuscript is a Massachusetts General Hospital (MGH) prototype distinct from that of CorTechs Laboratories. BF provides consulting services to CorTechs Laboratories. AvdK and BF are eligible to receive a portion of licensing fees paid to MGH by CorTechs Laboratories. FS and MH are employees of Siemens Medical Solutions.

* Corresponding author. Fax: +1 617 724 7422.
*E-mail address:* andre@nmr.mgh.harvard.edu (A.J.W. van der Kouwe).
**Available online on ScienceDirect (www.sciencedirect.com).**

1053-8119/$ - see front matter © 2005 Elsevier Inc. All rights reserved.
doi:10.1016/j.neuroimage.2005.03.035

reference are resolved within less than 5°. Welch et al. (2002) have proposed a method for alignment using rapidly acquired spherical navigator echoes. This method is fast and accurate but requires a reference navigator for each subject and is therefore ideally suited for automatic registration between scans of the same subject and not between scans of different subjects (Welch et al., 2004). Stereotactic systems have been used in MRI and CT to ensure a standard coordinate system for neurosurgical applications (Heilbrun et al., 1987; Kondziolka et al., 1992) but cannot be used in clinical routine because of the time-consuming and invasive nature of the procedure. A device worn like a pair of eyeglasses that supports fiducial markers visible in MR images has been proposed along with a registration algorithm (Oshio et al., 1996).

Solutions to the problem of off-line motion correction for between-volume correction are well-established (Cox and Jesmanowicz, 1999; Jenkinson and Smith, 2001). However, off-line motion correction is impractical in routine clinical practice as it requires additional processing time, results in an increased data amount, and introduces resampling artifacts. These artifacts are especially pronounced in the case of the highly non-isotropic voxels that are typical of clinical scans, making the comparison of resampled clinical volumes in longitudinal clinical studies less reliable. The quality of the registration itself is also confounded by the non-isotropic voxels. In our procedure, the alignment is based on a rapidly acquired 3D localizer scan with isotropic spatial resolution.

## Materials and methods

The procedure begins with a localizer scan during which two medium-resolution, large field-of-view scans of the head are acquired (3D gradient echo, TR = 2.2 ms, TE = 1.1 ms, bandwidth = 1070 Hz/pixel, flip angles = 2° and 6°, field of view = 320 mm, 2.5 mm isotropic resolution, 128 slices). By collecting two volumes with different contrasts, we are able to better separate tissue classes (gray matter, white matter, CSF) than would be possible with only a single contrast. Information relating tissue class to contrast is encoded in a pre-compiled statistical atlas, built from segmented brain images. The 3D localizer scans are registered using a rigid body alignment procedure to the atlas, which represents the anatomical variation

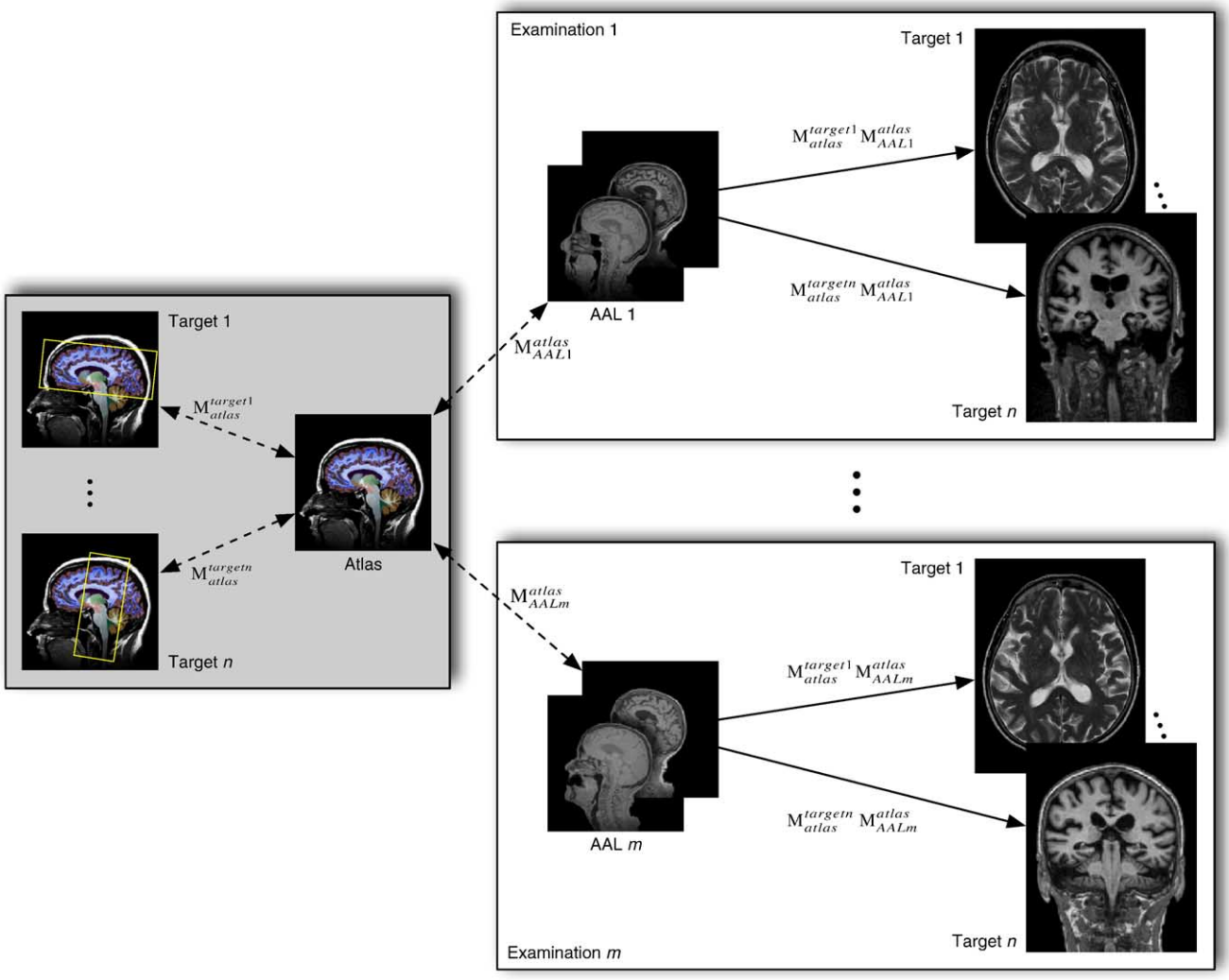


Fig. 1. Workflow for automatic scan positioning with matrices relating the target patient position within the scanned volume to the statistical atlas and automatic alignment localizer (AAL).

within a population of 40 healthy adult subjects (21 males, 19 females). The result of the alignment is a matrix representing the optimal registration of the subject to the atlas. This matrix is then used to define the slice position and orientation of subsequent scans during the same scanning session. A graphical representation of the procedure is shown in Fig. 1.

*Automatic alignment to probabilistic atlas*

The alignment procedure relies on a pre-compiled probabilistic atlas of aligned brain images. This atlas contains two types of information viz. the probability of a given tissue type (e.g. gray matter, white matter, CSF, skin, skull, eyes) occurring at a given location in atlas space and the conditional probability distribution of the multi-spectral MRI intensity values for a given tissue class. The atlas-based alignment procedure seeks to find the most probable alignment and tissue classification for the subject, given localizer scans and atlas information. This approach scales well with pathology, and the problem is highly overdetermined.

More formally, we seek to maximize the joint probability of an atlas function $f(\mathbf{r})$ and tissue classification $\boldsymbol{C}$, given the observed multi-spectral image $\boldsymbol{I}$:

$$p(\boldsymbol{C},f|\boldsymbol{I}) \propto p(\boldsymbol{I}|\boldsymbol{C},f)p(\boldsymbol{C}|f)p(f). \tag{1}$$

The atlas function $f(\mathbf{r})$ maps atlas coordinates into the corresponding points in the individual subject. The tissue classification vector $\boldsymbol{C}$ specifies the tissue class for each voxel location (see Fischl et al. (2002, 2004) for a more complete description of this approach). The terms $p(\boldsymbol{I}|\boldsymbol{C},f)$ and $p(\boldsymbol{C}|f)$ in Eq. (1) provide a natural means for incorporating atlas information into the segmentation procedure. The first term encodes the relationship between the class label at each atlas location and the predicted image intensities. Using the atlas space, we can allow the class statistics to vary as a function of location, allowing the within-class variations in tissue properties that are known to exist in the human brain (Cho et al., 1997; Steen et al., 2000) to be captured in a natural manner. The second term allows the expression of prior information regarding the spatial structure of the anatomical classes. Finally, the term $p(f)$ provides a means for constraining the space of allowable atlas functions (e.g. continuity, differentiability, and invertibility).

Here, the atlas mapping function is assumed to be a rigid-body transformation, i.e.

$$f(\mathbf{r}) = \mathbf{M}\mathbf{r} \tag{2}$$

where

$$\mathbf{M} = \begin{pmatrix} \cos\varphi\cos\phi + \sin\varphi\sin\theta\sin\phi & \sin\varphi\cos\theta & -\cos\varphi\sin\theta\sin\phi + \sin\varphi\cos\phi & t_x \\ -\sin\varphi\cos\theta & \cos\varphi\cos\theta & \sin\theta & t_y \\ \sin\varphi\sin\theta\cos\phi - \cos\varphi\sin\theta & -\cos\varphi\sin\theta - \sin\varphi\sin\theta & \cos\theta\cos\varphi & t_z \\ 0 & 0 & 0 & 1 \end{pmatrix}$$

The transformation matrix $\mathbf{M}$ is parameterized by three translations ($t_x$, $t_y$, and $t_z$) and three rotation angles ($\theta$, $\varphi$, and $\phi$). Furthermore, the a priori probability of all rigid body transformations is assumed to be uniform (i.e., $p(f)$ = const). We could have put priors on $\mathbf{M}$ given knowledge of the subject positions but did not do so as performance was satisfactory without this additional information. Thus, assuming (1) that the multi-spectral image intensities for a given tissue class $c$ can be represented by a multi-variate Gaussian distribution with mean $\mu_c$ and covariance matrix $\boldsymbol{\Lambda}_c$, and (2) voxel-wise independence of the noise, the optimal classification $\boldsymbol{C}$ and rigid-body registration matrix $\mathbf{M}$ is given by

$$\begin{aligned} \boldsymbol{C},\mathbf{M} &= \arg\min J_{\boldsymbol{C},\mathbf{M}} \\ &= \sum_i \Big( (\boldsymbol{I}(\mathbf{M}\mathbf{r}_i) - \mu_c)^T \boldsymbol{\Lambda}_c^{-1} (\boldsymbol{I}(\mathbf{M}\mathbf{r}_i) - \mu_c) - \log(p_c(\mathbf{r}_i)) \Big), \end{aligned} \tag{3}$$

where $\mathbf{r}_i$ range over locations within brain in atlas space, $c$ denotes the tissue classification, and $p_c(\mathbf{r}_i)$ denotes the a priori probability of tissue class $c$ at location $\mathbf{r}_i$, where $i$ is the index to a list of locations within the brain in atlas space. Since we vary only the 6 rigid body parameters in the acquisitions aligned using the calculated registration matrix, we solve only for these 6 parameters in the optimization, that is, we do not scale head size to match the atlas. This produces sufficiently accurate and more repeatable results and requires less time to compute than a non-rigid registration.

*Compilation of statistical atlas*

The statistical atlas for our implementation was compiled from a database of 40 subjects scanned using a high-resolution, multi-spectral protocol consisting of four separate scans (3D GRE, TR = 20 ms, $\alpha$ = 3°, 5°, 20°, 30°, resolution = 1 mm isotropic). Each subject's scans were aligned and segmented using the method described in Fischl et al. (2002), generalized for multi-spectral acquisitions (Fischl et al., 2004). The class statistics $\mu_c$ and covariance matrix $\boldsymbol{\Lambda}_c$ and $p_c(\mathbf{r})$ were then estimated for each tissue class based on these aligned and segmented (or tissue classified) cases. Note that, whereas the tissue class probability function $p_c(\mathbf{r})$ is strictly a function of the subject population (i.e. independent of the scanner or scan parameter used), the signal intensity mean $\mu_c$ and covariance matrix $\boldsymbol{\Lambda}_c$ depend on factors such as field strength, pulse sequence, and scan parameters.

Generalization of the atlas from the high-resolution multi-spectral protocol used to derive the class statistics to the fast, medium-resolution acquisition used as a localizer for the automatic alignment procedure was done by solving for "effective" tissue parameters ($T_1$ and proton density, $\rho_0$) using the closed form solution to the Bloch Equations for short TE, spoiled gradient echo sequences (Haacke et al., 1999):

$$\rho(\alpha, \mathrm{TR}, \rho_0, T_1) = \rho_0 \sin\alpha \frac{1 - e^{-\mathrm{TR}/T_1}}{1 - e^{-\mathrm{TR}/T_1}\cos\alpha}. \tag{4}$$

The same equation was then used to predict the relative image intensities for different tissue classes in the localizer scan by substituting the appropriate sequence parameters (TR and $\alpha$).

*Registration and offset matrices*

In an imaging study, the goal is to perform an examination $m$ at a specified target location $n$, with the target position predefined relative to an atlas (see Fig. 1). Let the registration matrix $\mathbf{M}$ of Eq. (3) be denoted by $\mathbf{M}_{\mathrm{atlas}}^{\mathrm{AAL}}$ (inverse of $\mathbf{M}_{\mathrm{AAL}}^{\mathrm{atlas}}$), the rigid body transformation that maps the brain of the statistical atlas to the subject's brain in the automatic alignment localizer (AAL). Subsequent routine clinical scans in the same session are aligned using the positioning determined by the AAL. An additional

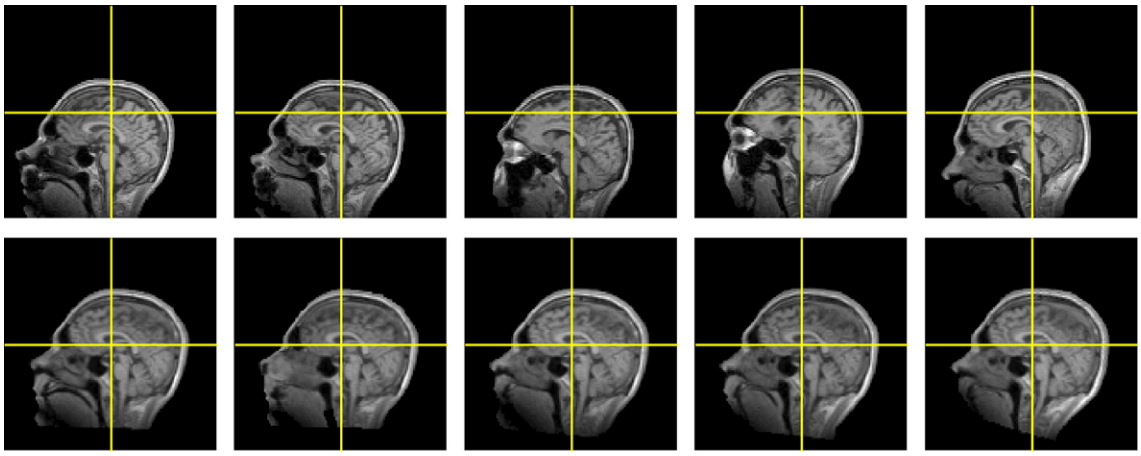

Fig. 2. Center slice of five medium resolution automatic alignment localizers of the same subject before (top line) and after (bottom line) automatic positioning. The volumes were resampled offline. The algorithm aligns the brain itself and disregards non-rigid anatomy such as lower jaw and neck.

fixed offset $\mathbf{M}_{\text{atlas}}^{\text{target}}$ may be applied, so that the patient is scanned at a predefined orientation relative to the atlas. The required orientation of the clinical scan relative to the orientation of the initial AAL is equal to the orientation of the target patient position relative to the AAL. It is calculated as follows:

$$\mathbf{M}_{\text{AAL}}^{\text{target}} = \mathbf{M}_{\text{atlas}}^{\text{target}}\,\mathbf{M}_{\text{AAL}}^{\text{atlas}} \tag{5}$$

*Implementation*

We have implemented a complete system following the workflow shown in Fig. 1 on the Siemens (Erlangen, Germany) 1.5 T Sonata, 1.5 T Symphony Quantum, 3 T Allegra, and 3 T Trio platforms, which incorporate different gradient coils and geometry. The automatic alignment localizer consists of two volumes with different flip angles in a single run of 42 s. The registration matrix $\mathbf{M}_{\text{AAL}}^{\text{atlas}}$ is calculated in 15 s (Intel Xeon, 1.8 GHz) and saved to disk.

In our implementation, each subsequent (automatically positioned) sequence that uses the matrix has been modified to use the automatic positioning matrix and to allow an offset relative to the atlas to be saved as part of the protocol. The automatically positioned sequences also have an additional feature – in-plane rotation – that was not previously available by default on the graphical user interface, that is, the technologist was unable to rotate the slab within the predominant slice plane using the default double-oblique positioning and therefore could not in principle

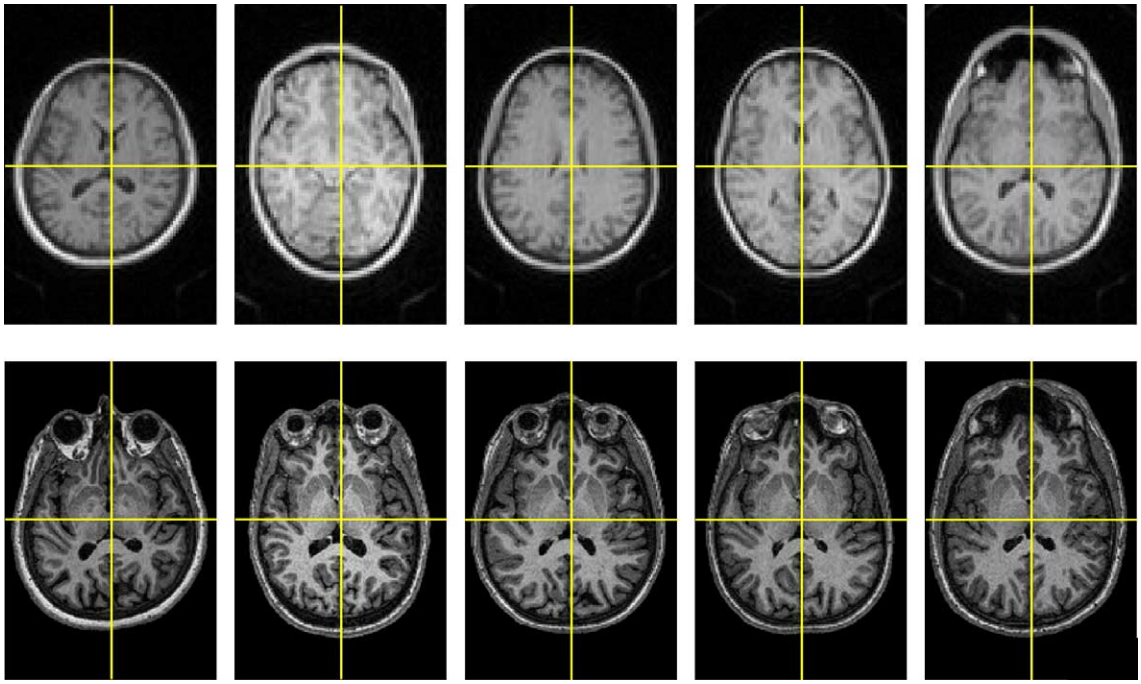

Fig. 3. Five axial images of the brains of five separate subjects, before automatic positioning (top row, automatic alignment localizer) and with automatic positioning (bottom row, MPRAGE). Corrections were performed on-line.

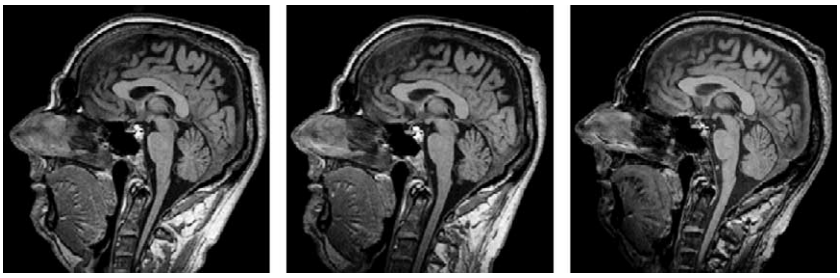

Fig. 4. Center slice of the same subject scanned with automatic positioning on Siemens Sonata (left), Symphony Quantum (center), and Trio (right) systems.

manually align the slice prescription perfectly as the automatic procedure is able to do.

## Results

We present results of automatic slice positioning with offsets applied in two ways. In the first, the target positioning is selected on a general atlas in order to scan all patients in a group with a standardized orientation. This is applicable in routine clinical brain imaging, cross-sectional research studies, and multi-subject longitudinal studies. We call this "atlas-based positioning," and setting the offset on the atlas is called "atlas-based planning". The offset is saved in a protocol specific to the study or type of examination. The second type of application is that in which the target positioning varies from patient to patient, depending on the specific pathology or structure of interest, but in this case, the requirement is to scan the same subject again during one or more follow-up sessions with exactly the same slice positioning. This is important for longitudinal studies of unique patients, and we call it "patient-based planning/positioning". The offset is saved in a protocol specific to the patient.

### *Atlas-based planning*

One approach to setting the target scan position would be to specify it graphically on the atlas image. However, our current implementation does not display the atlas, so planning (setting the offset rotations and translations) is done on any individual example subject and is then saved as part of the protocol. If this protocol is run after localizing other subjects, the planned positioning will be replicated in these subjects. Fig. 2 shows the middle slice of five AALs collected on the same subject in various positions (top row). The bottom row shows the middle slice of the same volumes resampled to match the default position of the atlas using the algorithm described earlier. The default atlas is positioned with the anterior–posterior commissure (AC–PC) line tilted at approximately 12°. It should be noted, however, that our algorithm aligns the brain and atlas globally and does not use landmarks such as the commissures. Whereas two-point registration with AC–PC is fundamental to Talairach registration and is used in stereotactic neurosurgery (Verard et al., 1997; Weiss et al., 2004), inter-rater reliability for detecting certain landmarks other than AC and PC after global registration has been shown to be better and therefore more appropriate in particular studies (Arndt et al., 1996; Johnson and Christensen, 2002). Fig. 3 shows a single scan from each of five different subjects before and after on-line prospective alignment with the default atlas. Again, notice good alignment to midline and right–left symmetry in the aligned images. Also visible is the close positioning of the slices from subject to subject. Fig. 4 shows the images of one subject after automatic alignment in Sonata, Symphony, and Trio scanners, respectively. Figs. 2–4 show that the brain as a whole is consistently aligned, while the non-rigid anatomy such as the spinal cord varies across the aligned images. In this report, we quantify only the performance of our prototype 1.5 T Sonata implementation.

Our clinical protocol is planned with an offset that places AC–PC approximately in the axial plane. The protocol includes automatically positioned versions of standard clinical sequences such as spin-echo, turbo spin-echo, gradient echo, FLAIR, and diffusion sequences. Preliminary results of a study in patients with brain tumors indicate that the consistency of automatic alignment is significantly better than that of the technologist (Benner et al., 2004). In the study, tumor patients were scanned with an axial TSE

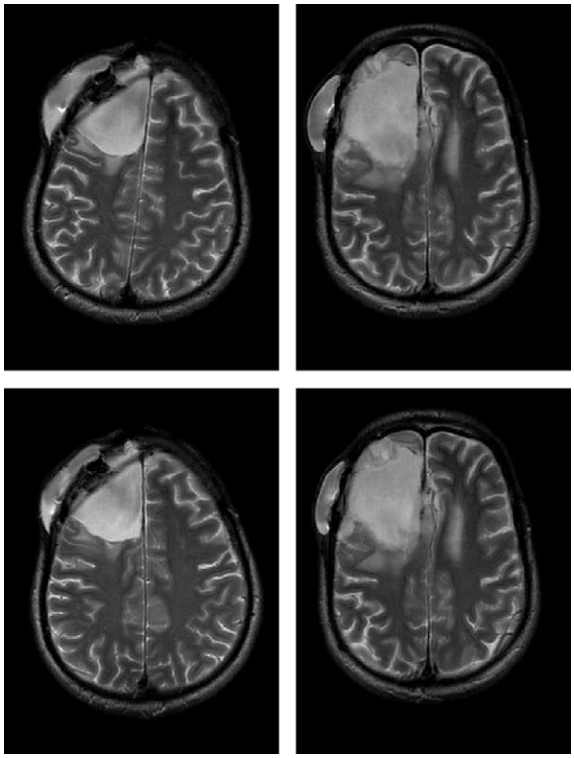

Fig. 5. Axial TSE of patient with tumor. Top left: aligned manually by technologist; top right: aligned automatically; bottom left: aligned manually by technologist on return visit; bottom right: aligned automatically on return visit. Note that the user interface did not allow the technologist to adjust the rotation in the acquisition plane (axial), and the technologist was therefore unable to correct the midline rotation errors reflected in the images on the left without repositioning the patient. In contrast, the automatic positioning algorithm was able to manipulate this parameter.

positioned by the technologist in the routine manner and aligned using the automatic positioning procedure. Patients returned a few weeks later for a repeat set of scans. Fig. 5 shows test–retest positioning by the technologist on the left and automatic test–retest positioning on the right for an example patient.

*Patient-based planning*

Whereas atlas-based planning results in a single protocol that is applied to all patients, patient-based planning results in a protocol specific to an individual patient. This method may be applied to

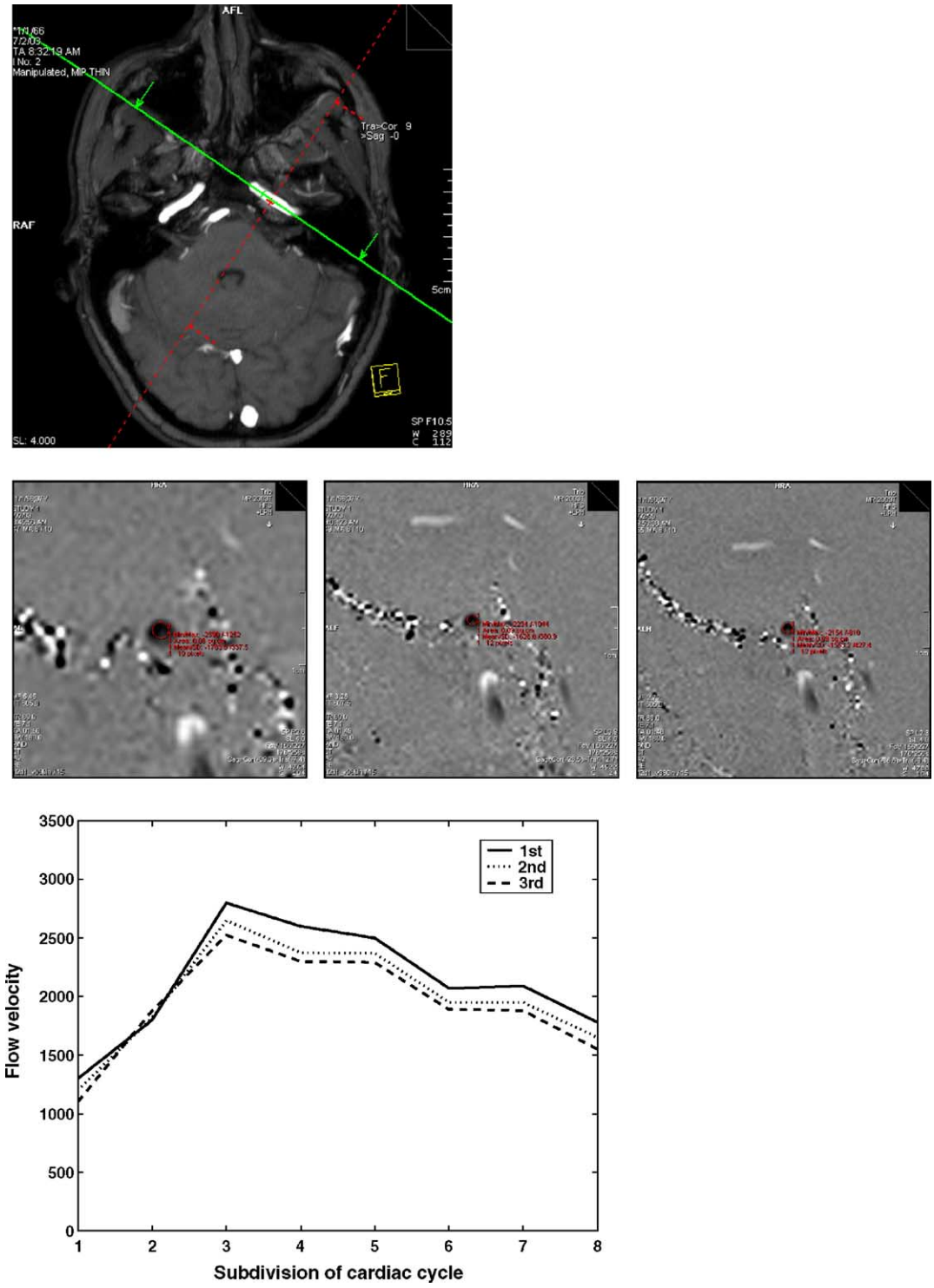


Fig. 6. Top: flow measurement planned on anatomical maximum intensity projection; middle: phase images for each of three velocity measurements automatically aligned without repeated planning (subject left patient table momentarily between scans, first image after planning is magnified); bottom: flow measurements across cardiac cycle for each of three acquisitions (flow velocity in arbitrary units vs. uniform divisions in time across cardiac cycle).

patients with specific localized pathologies, such as tumors. In both atlas- and patient-based planning, alignment is calculated with respect to the standard atlas, therefore no reference data need to be stored for the patient.

The patient-based method has been applied to plan angiographic scans of individual migraine subjects. In these patients, it is critical to obtain blood flow measurements at short notice during an acute event, and it is therefore useful to be able to plan the scan in advance. The vessel of interest is identified in a maximum intensity projection angiography image during a first visit. The slice for through-plane velocity encoded imaging is positioned perpendicular to the vessel as shown in Fig. 6 (top). A first velocity encoded scan is performed using this positioning, and the phase image is shown in Fig. 6 (middle) with the vessel marked. The orientation of this slice relative to the atlas is saved in a patient-specific protocol. Using this protocol, the subject can now be rescanned on a later occasion without the need to reacquire the anatomical volume or replan the positioning of the velocity encoded scan. Fig. 6 (middle) shows the phase images acquired with automatic positioning after having the subject leave and return to the scanner twice. Fig. 6 (bottom) suggests that the flow measurements are reproduced accurately by the automatically positioned scans, without repeated planning.

Another application where patient-based planning may be useful is in longitudinal spectroscopic studies of patients. In such studies, it is important to place the volume over which the spectrum is acquired in exactly the same part of the brain during each follow-up visit. Even though the overall size of the brain varies from subject to subject and the position of the pathology varies from one subject to another, atlas-based automatic alignment is useful if the offset in positioning relative to the atlas is saved separately for each subject.

### *Quantification of performance*

We studied the test–retest performance of our implementation of the automatic registration procedure in a set of ten healthy volunteers. Each subject was scanned on two separate occasions with both the automatic alignment localizer and a whole-brain MPRAGE scan automatically positioned using the localizer. The individual results are shown in Tables 1 and 2, and the performance is summarized in Table 3.

Table 1
Intrasubject results for automatic alignment localizers

| Translation [mm] | | | Rotation [degrees] | | | MSE (before AA) | MSE (AA) |
|---|---|---|---|---|---|---|---|
| $x$ | $y$ | $z$ | $\theta$ | $\varphi$ | $\phi$ | | |
| −0.14 | −0.73 | 2.45 | 0.70 | 0.40 | 0.21 | 92.40 | 33.86 |
| −0.60 | 0.01 | −0.51 | 1.40 | −0.34 | 0.40 | 74.00 | 31.73 |
| −0.15 | −0.25 | 0.25 | 0.34 | −0.55 | 0.41 | 68.04 | 25.03 |
| 0.25 | 0.20 | −0.05 | −0.55 | 0.36 | −1.25 | 71.65 | 22.29 |
| −0.05 | −0.25 | 0.20 | −0.10 | 0.05 | −0.30 | 60.61 | 14.47 |
| 0.20 | −0.65 | 0.17 | 0.05 | −1.00 | 0.15 | 69.52 | 24.98 |
| 0.10 | 0.56 | 0.55 | −0.05 | −0.50 | −0.20 | 61.17 | 18.76 |
| 0.10 | −0.40 | 0.40 | 0.08 | −0.80 | −1.00 | 60.14 | 19.59 |
| 0.10 | 0.41 | 0.69 | 0.05 | 0.55 | 0.10 | 65.20 | 19.04 |
| 0.20 | −0.05 | 0.70 | −0.15 | 0.05 | 0.10 | 64.85 | 21.63 |

Individual translations and rotations between automatic alignment localizers used to position intrasubject MPRAGE volumes, compared using Matlab image registration between T1-weighted (6°) volumes of localizers. Mean square errors (MSE) are listed for the localizers as acquired and after resampling to the automatically determined alignment (residual error reflects non-rigid anatomy).

Table 2
Intrasubject results for MPRAGE volumes

| Translation [mm] | | | Rotation [degrees] | | | MSE (AA) | MSE (AA + FLIRT) |
|---|---|---|---|---|---|---|---|
| $x$ | $y$ | $z$ | $\theta$ | $\varphi$ | $\phi$ | | |
| 0.87 | −2.61 | −0.62 | 0.40 | 0.61 | 0.27 | 88.44 | 60.91 |
| 3.24 | −0.89 | −2.04 | −0.37 | 1.42 | 0.06 | 67.32 | 52.10 |
| 2.33 | −1.68 | −0.80 | −0.78 | 0.35 | −0.11 | 60.87 | 51.09 |
| 0.15 | −0.07 | 0.27 | 0.11 | −0.05 | −0.07 | 47.85 | 37.95 |
| −1.97 | 0.53 | 2.72 | 0.86 | −0.51 | 0.49 | 62.00 | 38.59 |
| 3.37 | −2.82 | −0.60 | −1.10 | 0.10 | −0.13 | 63.36 | 50.42 |
| −0.81 | −0.06 | 0.49 | 0.07 | −0.06 | 0.23 | 49.33 | 41.46 |
| 2.10 | −0.14 | −3.60 | −0.79 | 0.36 | −1.03 | 56.58 | 42.01 |
| −3.13 | 4.26 | −4.01 | 1.31 | 0.46 | −0.80 | 61.56 | 42.20 |
| −2.63 | 1.81 | 0.39 | 0.90 | −0.53 | −0.14 | 62.05 | 45.92 |

Individual translations and rotations between MPRAGE volumes collected with automatic positioning, and compared using FLIRT, along with MSE between volumes before and after registration with FLIRT. Mean square errors (MSE) are listed for the automatically positioned MPRAGEs and for the MPRAGEs resampled using the registration matrix generated by FLIRT.

Since the residual errors for the MPRAGE include errors due to post-localizer motion of the subject, we first tested the algorithm directly by comparing the localizer volumes. We resampled the localizers using the rotation and positioning determined by the automatic alignment algorithm (to match the orientation of the MPRAGE scans). FLIRT (Jenkinson and Smith, 2001) did not perform well on these volumes, possibly because of the lower resolution and low contrast of the volumes, so we applied our own matching algorithm (distinct from the automatic positioning algorithm) implemented using Matlab (The MathWorks, Natick, Massachusetts) that does a simple fit between the intensities of the two high flip angle (T1-weighted) volumes, embedded in a multiscale search that finds the residual difference in orientation that results in the minimum mean square error in intensities between the two volumes. Individual results are listed in Table 1. The minimum, maximum, and mean square residual errors in the translations and rotations for the localizer pairs and MPRAGE pairs are listed in Table 3.

In principle, the pairs of MPRAGE volumes for the same subject scanned during two separate sessions should be aligned precisely except for the distortions due to gradient non-linearities and B0 inhomogeneities. To gauge the error on the

Table 3
Summary of intrasubject (test–retest) results for ten subjects

| | | Translation [mm] | | | Rotation [degrees] | | |
|---|---|---|---|---|---|---|---|
| | | $x$ | $y$ | $z$ | $\theta$ | $\varphi$ | $\phi$ |
| AAL | min. | −0.60 | −0.73 | −0.51 | −0.55 | −1.00 | −1.25 |
| | max. | 0.25 | 0.56 | 2.45 | 1.40 | 0.55 | 0.41 |
| | m.s. | 0.24 | 0.42 | 0.89 | 0.54 | 0.54 | 0.56 |
| MPRAGE | min. | −3.13 | −2.82 | −4.01 | −1.10 | −0.53 | −1.03 |
| | max. | 3.37 | 4.26 | 2.72 | 1.31 | 1.42 | 0.49 |
| | m.s. | 2.32 | 2.00 | 2.06 | 0.78 | 0.58 | 0.46 |

Residual differences (minimum, maximum, mean square) in translations and rotations of resampled automatic alignment localizer (AAL) and automatically positioned MPRAGE. These results reflect not only inaccuracies in the automatic alignment, but also errors in the offline registration algorithms.

Table 4
Summary of intersubject results for two groups of ten subjects

| | | Translation [mm] | | | Rotation [degrees] | | |
|---|---|---|---|---|---|---|---|
| | | $x$ | $y$ | $z$ | $\theta$ | $\varphi$ | $\phi$ |
| MPRAGE (manual) | min. | −47.48 | −51.85 | −12.46 | −23.81 | −3.33 | −3.92 |
| | max. | 59.14 | 98.08 | 18.53 | 30.88 | 3.33 | 5.39 |
| | m.s. | 28.73 | 33.18 | 6.11 | 12.02 | 1.51 | 2.15 |
| MPRAGE (automatic) | min. | −20.47 | −16.51 | −6.20 | −7.73 | −1.63 | −2.05 |
| | max. | 27.91 | 8.46 | 2.87 | 3.88 | 1.97 | 1.31 |
| | m.s. | 9.00 | 6.58 | 2.28 | 2.50 | 0.71 | 0.81 |
| $P$ value | | 0.0503 | <0.0001 | 0.0019 | 0.0032 | 0.1075 | 0.6605 |

Comparison of each subject with all others in groups of ten (45 comparisons) using FLIRT for manually positioned vs. automatically positioned subjects. Shown are minimum, maximum, and mean square of translations and rotations. Some residual error are due to FLIRT attempting to register non-rigid parts of the anatomy.

MPRAGE, we used FLIRT to register the already automatically aligned volumes. To test the null hypothesis that registration using FLIRT does not further improve registration over what automatic positioning achieves, we calculated the MSE between the two automatically positioned volumes, and the MSE between these volumes resampled using FLIRT's alignment. A paired $t$ test comparing these sets yields a $P$ value of smaller than 0.001, and we thus conclude that FLIRT further improves the registration calculated by the automatic positioning algorithm. There are two sources of inaccuracy in the automatic positioning of the MPRAGE. The first is inaccuracies in the automatic positioning algorithm. The second is subject motion after the localizer but before or during the long (8 min) MPRAGE scan. Motion during the automatic alignment localizer will also affect the quality of the alignment, although this scan is only 42 s long. Whereas automatic registration uses the two volumes of the localizer to distinguish brain from non-rigid tissue, FLIRT has only the intensity values in the MPRAGE to use for matching. To decrease the bias introduced when FLIRT tries to align non-rigid tissue (e.g. lower jaw, tongue, neck), we mask the brains with a spherical mask during registration. We also calculate the MSE in the masked region only.

Another important aspect of the automatic positioning algorithm is its ability to align the brains of different subjects with one another. We scanned ten subjects with automatically positioned whole-brain MPRAGEs and ten different subjects with manually prescribed MPRAGEs. We used FLIRT to detect the residual translation and rotation errors between each combination of pairs of scans within the ten-subject pool (45 combinations). Table 4 shows the minimum, maximum, and mean square translation and rotation differences for the manually prescribed and automatically positioned MPRAGEs, respectively. These results may also reflect inaccuracies in our application of the FLIRT algorithm, in particular because FLIRT attempts to register the non-rigid anatomy in the head. In this case, spherical masking is complicated by the fact that the brains are not necessarily centered in the middle of the volume, so we did not apply any mask.

To test whether automatic alignment reduces the variability of alignment achieved by manual positioning, we use the $F$ test to compare the variances on the rotations and translations of the manual vs. automatically positioned MPRAGEs. The resulting $P$ values for all translation directions and rotation axes are listed in Table 4. The much better performance in rotation about the $x$ axis (left–right) may be accounted for by the fact that this axis is perpendicular to the scanning plane (sagittal) and the user interface does not allow manual setting of rotations about this axis (in-plane rotation), whereas the automatic method is able to set arbitrary in-plane rotations. If we use Fisher's method to combine the $P$ values (Snedecor and Cochran, 1989), we conclude that the variance of the overall test–retest is improved by automatic positioning ($P < 0.001$), despite the bias against automatic positioning introduced because FLIRT attempts to align non-rigid anatomy.

## Discussion

Our results indicate that automatic alignment significantly improves the consistency of inter-subject positioning and suggest that it improves test–retest consistency in positioning with follow-up scans of the same subject. The procedure is currently being used in several research studies at our hospital and elsewhere.

Because changes in the subject's position subsequent to the localizer will introduce errors in the positioning of later scans, we are developing an automated correction procedure that will ensure consistent alignment between volumes acquired in the same session, using a short reference scan collected immediately after the initial automatic alignment localizer. Motion correction schemes using embedded navigators for tracking and correcting for motion within long high resolution anatomical scans have been suggested (Van der Kouwe and Dale, 2004; Ward et al., 2000; Welch et al., 2002). In future work, we therefore hope to address consistency in positioning between and within the scans of a single automatically positioned session. Welch et al. (2002, 2004) have developed a technique for interscan registration using rapidly acquired spherical navigators. Their technique may also be used to align scans between sessions, but in this case, a reference needs to be stored for each individual subject. In principle, the alignment should be more accurate if the reference is specific to the individual rather than an average atlas. However, the advantage of using an atlas is that reproducible prescriptions can always be performed, even in cases when a subject-specific reference is not available, including at a different scanner at another location or at a scanner of a different type.

The choice and number of example brains used to build our atlas limits our implementation. In particular, young children's brains and brains with resected anatomy are more challenging to the algorithm and result in poorer alignment. In this case, a modified atlas would be needed for automatic alignment, or a

technique using an individual reference would have to be used to register between sessions. The same is true for other body parts such as the knee or heart, although in these cases the non-rigid nature of the anatomy represents a further challenge.

We expect that the use of automatic prospective scan positioning will result in more consistent clinical scanning, not only within a site, but also between scanners and between sites. We also expect that automatic positioning will contribute to improved care in patients where follow-up scans are necessary to monitor progress in response to treatment. Automatic positioning has already contributed to consistent scanning in several longitudinal studies at our institution.

## Acknowledgments

We thank Dr. Mark Vangel for assistance with the statistics, Dr. Chris Wiggins and Dr. Nouchine Hadjikhani for assistance with velocity encoded scans, and Dr. Jonathan Wisco for clinical data. This work was supported in part by NIBIB R21EB02530, NCRR P41RR14075, RO1 RR16594-01A1, NCRR BIRN Morphometric Project BIRN002, RO1-EB1550, the Mental Illness and Neuroscience Discovery (MIND) Institute, and Siemens Medical Solutions.

## References

Arndt, S., Rajarethinam, R., Cizadlo, T., O'Leary, D., Downhill, J., Andreasen, N.C., 1996. Landmark-based registration and measurement of magnetic resonance images: a reliability study. Psychiatry Res. 67 (2), 145–154.

Benner, T., Wisco, J.J., van der Kouwe, A., Fischl, B., Sorensen, A.G., 2004. Accuracy and repeatability of automatic slice positioning compared with manual slice positioning. 12th Meeting of the ISMRM, Kyoto, Japan, May.

Cho, S., Jones, D., Reddick, W.E., Ogg, R.J., Steen, R.G., 1997. Establishing norms for age-related changes in proton T1 of human brain tissue in vivo. Magn. Reson. Imaging 15 (10), 1133–1143.

Cox, R.W., Jesmanowicz, A., 1999. Real-time 3D image registration for functional MRI. Magn. Reson. Med. 42, 1014–1018.

Fischl, B., Salat, D.H., Busa, E., Albert, M., Dietrich, M., Haselgrove, C., van der Kouwe, A., Killiany, R., Kennedy, D., Klaveness, S., Montillo, A., Makris, N., Rosen, B., Dale, A.M., 2002. Whole brain segmentation: automated labeling of neuroanatomical structures in the human brain. Neuron 33, 341–355.

Fischl, B., Salat, D.H., van der Kouwe, A.J., Makris, N., Segonne, F., Quinn, B.T., Dale, A.M., 2004. Sequence-independent segmentation of magnetic resonance images. NeuroImage 23 (Suppl. 1), S69–S84.

Freeborough, P.A., Woods, R.P., Fox, N.C., 1996. Accurate registration of serial 3D MR brain images and its application to visualizing change in neurodegenerative disorders. J. Comput. Assist. Tomogr. 20 (6), 1012–1022.

Haacke, E.M., Brown, R.W., Thompson, M.R., Venkatesan, R., 1999. Magnetic Resonance Imaging: Physical Principles and Sequence Design. John Wiley and Sons, New York.

Heilbrun, M.P., Sunderland, P.M., McDonald, P.R., Wells, T.H., Cosman, E., Ganz, E., 1987. Brown–Roberts–Wells stereotactic modifications to accomplish magnetic resonance imaging guidance in three planes. Appl. Neurophysiol. 50, 143–152.

Itti, L., Chang, L., Ernst, T., 2001. Automatic scan prescription for brain MRI. Magn. Reson. Med. 45 (3), 486–494.

Jenkinson, M., Smith, S., 2001. A global optimization method for robust affine registration of brain images. Med. Image Anal. 5 (2), 143–156.

Johnson, H.J., Christensen, G.E., 2002. Consistent landmark and intensity-based image registration. IEEE Trans. Med. Imaging 21 (5), 450–461.

Kondziolka, D., Dempsey, P.K., Lunsford, L.D., Kestle, J.R., Dolan, E.J., Kanal, E., Tasker, R.R., 1992. A comparison between magnetic resonance imaging and computed tomography for stereotactic coordinate determination. Neurosurgery 30 (3), 402–407.

Molyneux, P.D., Tofts, P.S., Fletcher, A., Gunn, B., Robinson, P., Gallagher, H., Moseley, I.F., Barker, G.J., Miller, D.H., 1998. Precision and reliability for measurement of change in MRI lesion volume in multiple sclerosis: a comparison of two computer assisted techniques. J. Neurol., Neurosurg. Psychiatry 65 (1), 42–47.

Oshio, K., Panych, L.P., Guttman, C.R., 1996. A simple noninvasive stereotactic device for routine MR head examinations. J. Comput. Assist. Tomogr. 20 (4), 588–591.

Snedecor, G.W., Cochran, W.G., 1989. Statistical Methods, eighth ed. Iowa State Univ. Press.

Steen, R.G., Reddick, W.E., Ogg, R.J., 2000. More than meets the eye: significant regional heterogeneity in human cortical T1. Magn. Reson. Imaging 18 (4), 361–368.

Van der Kouwe, A., Dale, A., 2004. Rapid real-time prospective rigid body motion correction during imaging using clover-leaf navigators. 12th Meeting ISMRM, Kyoto, Japan, May, 95.

Verard, L., Allain, P., Travere, J.M., Baron, J.C., Bloyet, D., 1997. Fully automatic identification of AC and PC landmarks on brain MRI using scene analysis. IEEE Trans. Med. Imaging 16 (5), 610–616.

Ward, H.A., Riederer, S.J., Grimm, R.C., Ehman, R.L., Felmlee, J.P., Jack, C.R., 2000. Prospective multiaxial motion correction for fMRI. Magn. Reson. Imaging 43 (3), 459–469.

Weiss, K.L., Storrs, J., Weiss, J.L., Strub, W., 2004. CT brain prescriptions in Talairach space: a new clinical standard. Am. J. Neuroradiol. 25 (2), 233–237.

Welch, E.B., Manduca, A., Grimm, R.C., Ward, H.A., Jack, C.R., 2002. Spherical navigator echoes for full 3D rigid body motion measurement in MRI. Magn. Reson. Med. 47 (1), 32–41.

Welch, E.B., Manduca, A., Grimm, R.C., Jack, C.R., 2004. Interscan registration using navigator echoes. Magn. Reson. Med. 52 (6), 1448–1452.